Competition between Jahn-Teller coupling and orbital fluctuations in $HoVO_3$

G. R. Blake,[1,*] A. A. Nugroho,[2] M. J. Gutmann,[3] and T. T. M. Palstra[1]
[1]*Solid State Chemistry Laboratory, Zernike Institute for Advanced Materials, University of Groningen, Nijenborgh 4, 9747 AG Groningen, The Netherlands*
[2]*Jurusan Fisika, Institut Teknologi Bandung, Jl. Ganesha 10, Bandung 40132, Indonesia*
[3]*ISIS Facility, Rutherford Appleton Laboratory-STFC, Chilton, Didcot, Oxfordshire OX11 0QX, United Kingdom*
(Received 3 October 2008; published 5 January 2009)

We have carried out a detailed study of the structural properties of $HoVO_3$ perovskite using a combination of single-crystal neutron diffraction and synchrotron x-ray and neutron powder diffraction. We focus on the competition between one-dimensional fluctuations of the occupied vanadium *d* orbitals and coherent Jahn-Teller distortion due to long-range orbital ordering. At room temperature orbital fluctuations are dominant. Below 188 K a structural phase transition from orthorhombic *Pbnm* to monoclinic *Pb*11 symmetry takes place, corresponding to a state where strong orbital fluctuations are superimposed on an underlying orbitally ordered state. However, the fluctuations are not strong enough to give rise to a long-range orbitally dimerized state as theoretically predicted. Ordering of the vanadium spins at 114 K has little effect on the orbital fluctuations, but the orbital ordering becomes coherent below a first-order transition to an orthorhombic *Pbnm* phase at 40 K.

DOI: 10.1103/PhysRevB.79.045101 PACS number(s): 71.70.Ej, 61.05.cp, 61.05.fm, 61.50.Ks

I. INTRODUCTION

The RVO_3 compounds (R=rare earth or Y) are highly distorted perovskites that have attracted attention in recent years due to their complex interplay between spin and orbital ordering (OO) often manifested by multiple phase transitions.[1–7] These materials contain V^{3+} in octahedral coordination, and thus three t_{2g} orbitals are occupied by two electrons. Electronic energy can be gained by lifting this orbital degeneracy via the Jahn-Teller (JT) effect—a cooperative distortion of the VO_6 octahedra that results in an ordered occupation of the orbitals below a so-called OO temperature T_{OO}. The second-order phase transition at T_{OO} is clearly visible in specific-heat measurements of RVO_3, which have shown that T_{OO} increases across the rare-earth series from ~140 K for $LaVO_3$ to a maximum of ~210 K at $GdVO_3$ before decreasing to ~170 K at $LuVO_3$.[5] Antiferromagnetic (AF) ordering of the V spins takes place below T_{OO} for all R except La at temperatures decreasing from T_N=142 K for $LaVO_3$ (Ref. 8) to 105 K for $LuVO_3$.[9] For R with smaller ionic radius than Dy, a first-order structural phase transition to an OO state of different symmetry, together with a spin reorientation, takes place at a temperature T_S that is well below T_N. For intermediate R a partial transition can take place and a coexistence of the two different OO configurations can be stabilized down to low temperature.[10]

In RVO_3 the V d_{xy} orbitals are always lowest in energy due to their direct overlap with the 2*p* orbitals of the oxygen ligands, and thus they are expected to be occupied most favorably in the OO state. In the simplest scenario the remaining V *d* electron occupies either the d_{xz} or d_{yz} orbital depending on the local distortion of the octahedron, which can give rise to two possible OO configurations. The so-called *G*-type OO always sets in on cooling through T_{OO}, where an alternating or "antiferro-" occupation of the d_{xz} and d_{yz} orbitals is found along all three crystal axes. A different configuration is present in the ground state when the octahedral tilting is large, that is, for R smaller than Dy. Here the orbital occupation is antiferro within the *ab* plane and "ferro" in the *c* direction and is known as *C*-type OO. The *C*-type configuration is considered in the literature to be well-defined with fully polarized orbitals and is consistent with orthorhombic *Pbnm* crystal symmetry. However, there is considerable disagreement about the nature of the *G*-type OO state. In particular, there is debate about whether the full degeneracy of the t_{2g} manifold is lifted at T_{OO} or whether partial orbital degeneracy remains down to T_N or lower temperatures.

A series of recent experiments has suggested that the *G*-type OO state is extremely complex in nature. Following the classical Goodenough-Kanamori-Anderson (GKA) rules,[11] the antiferro arrangement of the occupied orbitals along *c* in the ideal *G*-type OO state is consistent with ferromagnetic (FM) superexchange of V spins in this direction, which is experimentally observed. However, inelastic neutron scattering has shown that the ferromagnetic exchange along *c* is much stronger than the in-plane AF exchange; from the GKA rules it should be weaker. Furthermore, the ordered magnetic moment is only of the order of $1\mu_B$ (Refs. 4 and 12–14) compared to the spin-only value of $2\mu_B$ expected for an S=1 system. Other unexpected phenomena have been observed in the *G*-type phase. The magnon spectrum is split into optical and acoustic branches, suggesting that two FM interactions of different strengths are present along *c*.[13] Pronounced anisotropy in the optical conductivity could not be accounted for by the ideal *G*-type OO picture.[15–17] Infrared spectroscopy, extended x-ray-absorption fine structure (EXAFS) measurements,[18] and thermal conductivity[19] have pointed to the existence of structural disorder and "glassy" phonon behavior. Taken together, these pieces of experimental evidence can largely be explained by a picture where quantum fluctuations of the occupied orbitals occur along *c*.[20–24] When the fluctuations are strong the JT coupling is completely suppressed and total degeneracy of the *xz* and *yz* orbitals remains below T_{OO}. The degeneracy can be lifted if the *xz* and *yz* orbitals form a singlet that spans two adjacent V sites. Ordered chains of orbital singlets along *c* would then give rise to both a lattice distortion and to the

 ©2009 The American Physical Society

presence of alternating weak and strong FM interactions.[23] Although orbital excitations have been directly observed in the Raman spectra of $LaVO_3$, $NdVO_3$,[25] and YVO_3,[26] direct experimental evidence for an orbitally dimerized state is currently lacking and there is disagreement over the relative strengths of the competing orbital fluctuations and JT coupling and over the temperature range where each has most influence.[19,26–28] The situation is also likely to depend on the changing degree of octahedral tilting across the RVO_3 series.[29,30]

Orbital dimerization is expected to induce a small structural distortion involving alternating long and short V-V distances.[21] Therefore, it should be possible to investigate the presence of orbital dimerization using symmetry considerations. The room-temperature symmetry of all reported RVO_3 materials is orthorhombic *Pbnm*. On cooling through T_{OO}, diffraction experiments have suggested that a lowering of the crystal symmetry to monoclinic $P2_1/b11$ takes place for R=La,[31,32] Ce,[32] Nd,[14] Tb,[14] and Y (Ref. 4); in the case of Yb and Lu this transition has been reported to take place below T_N,[33,34] in contradiction to specific-heat measurements.[5] The structural transition involves the removal of mirror planes perpendicular to c at $z=\frac{1}{4}$ and $z=\frac{3}{4}$, the result of which is to render the two V-O "planes" at $z=0$ and $z=\frac{1}{2}$ crystallographically inequivalent. At the same time, the VO_6 octahedra distort in the ab plane such that each V atom has two "long" and two "short" V-O distances differing by up to 3.5%, while the V-O distance along c is little different to that in the room-temperature *Pbnm* phase. The observation of this bonding pattern has been interpreted as a signature of a cooperative JT effect and hence long-range G-type OO. However, the $P2_1/b11$ space group does not allow orbital dimerization to take place since the V atoms lie on special positions at $z=0$ and $z=\frac{1}{2}$. In the case of YVO_3, far-infrared vibrational spectroscopy showed that extra modes appear below T_{OO} that can only be explained by symmetry lower than $P2_1/b11$,[35] with the authors proposing either the monoclinic subgroup $Pb11$ or the triclinic subgroup $P\bar{1}$. In $Pb11$ the inversion symmetry along the b and c directions is removed and thus orbital dimerization is allowed along c. In $P\bar{1}$ the number of crystallographically distinct V atoms is increased from two to four, but they are still fixed on special positions and hence dimerization is not allowed.

There is a general lack of accurate structural information on the symmetry and bonding patterns in RVO_3 on which to base further experimental and theoretical works. We have therefore carried out a detailed structural study of $HoVO_3$ (the Ho^{3+} cation is slightly smaller than Y^{3+}) using a combination of synchrotron x-ray powder diffraction (XRPD) and both powder and single-crystal neutron diffractions. We show that the G-type OO of the intermediate phase in $HoVO_3$ is significantly perturbed by orbital fluctuations. However, despite the symmetry being lowered to $Pb11$, coherent orbital dimerization is not achieved.

II. EXPERIMENT

Single-crystal rods were grown using the floating-zone method described previously.[4] The oxygen content of a crushed piece of the crystal was determined by thermogravimetric analysis (TGA) using a Rheometric Scientific STA 1500. The weight gain was measured on heating the sample in air to 800 °C, where it was completely oxidized to $HoVO_4$. Assuming equal quantities of Ho and V, the stoichiometry of the sample was determined as $HoVO_{3.05(2)}$, which suggests the presence of a small deficiency of Ho or V. Magnetic-susceptibility measurements on an oriented single crystal were performed using a Quantum Design MPMS-7 superconducting quantum interference device (SQUID) magnetometer. Single-crystal neutron diffraction was carried out on the SXD beamline at the ISIS facility, which utilizes the time-of-flight Laue technique. A piece of the rod cut to a cube of approximate dimension 4 mm was attached to a sample stick and loaded into a closed-cycle refrigerator; data were collected at 20, 70, 140, and 295 K. The three-dimensional array of detectors allows a large volume of reciprocal space to be accessed in a single measurement. The sample stick was rotated by 180° in steps of 30° to obtain redundancy in each data set. Corrections for sample absorption and extinction were applied during the data reduction process at the beamline. Part of the crystal rod was crushed and neutron powder diffraction data were collected on the HRPD instrument at ISIS. A sample of mass 5 g was placed in a cylindrical vanadium can and cooled using a helium-cooled cryostat; data were collected at 5 K. Synchrotron XRPD data were collected on beamline ID31 at the European Synchrotron Radiation Facility (ESRF) using an incident wavelength of 0.4958 Å (25.01 keV). The sample was loaded into a quartz capillary and measurements were performed in the temperature range of 15–295 K using a helium-cooled cryostat. Structural refinements were carried out using the GSAS software suite[36] for both the powder and single-crystal data.

III. RESULTS

Magnetic-susceptibility data collected after zero-field cooling an oriented crystal piece and heating in an applied field of 50 Oe are shown in Fig. 1. The large paramagnetic signal from Ho tends to overshadow the anomalies that arise from the magnetic transitions involving the V spins when data are collected in higher measuring fields. The onset of canted AF ordering of the V spins can clearly be seen at T_N=114 K, below which the a-axis susceptibility is much larger than that of the other two axes. This is consistent with a small net FM moment along a that arises from slight canting of the V spins, as previously observed in YVO_3.[2] The discontinuous transition at T_S=40 K is analogous to the first-order transition at 77 K in YVO_3 and involves a change in the type of orbital ordering, as discussed below. The rapid increase in the a-axis susceptibility below ~10 K is consistent with an increased degree of ordering of the Ho spins; our neutron diffraction data (discussed below) show that the Ho spins have a rather strong FM component parallel to a and an AF component parallel to b. The Ho AF component is reflected in the maximum in the b-axis susceptibility at ~10 K. In contrast to YVO_3,[2] we did not observe any signature of T_{OO} in the high-temperature inverse susceptibility.

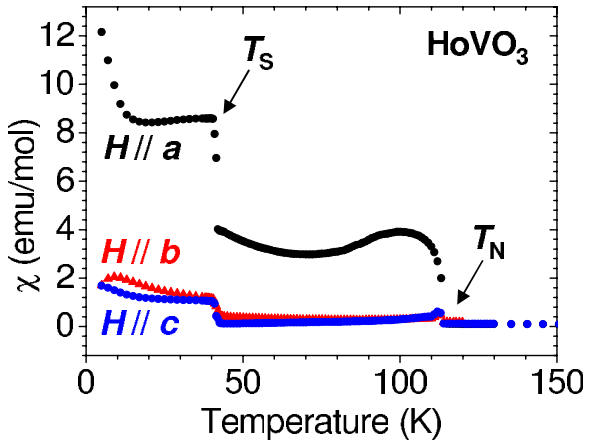

FIG. 1. (Color online) Zero-field-cooled magnetic susceptibility of $HoVO_3$ measured while heating in an applied field of 50 Oe along the three crystallographic axes. The structural phase transition at T_S and the magnetic ordering temperature T_N are indicated.

This is probably because the large paramagnetic moment of Ho^{3+} ($\sim 10.4\mu_B$) masks the much smaller signal from the V^{3+} sublattice. A similar observation has previously been made for $GdVO_3$ (Gd^{3+} has a moment of $\sim 7.9\mu_B$).[37]

The lattice parameters determined from the synchrotron XRPD data are shown in Fig. 2. The diffraction patterns down to 188 K could be well fitted using *Pbnm* symmetry, below which a lowering of symmetry from orthorhombic to monoclinic takes place, evidenced by the splitting of Bragg peaks that contain nonzero k and l Miller indices, as shown in Fig. 3. The symmetry of the monoclinic phase cannot be determined unambiguously from these data since apart from the splitting of existing peaks, no extra reflections were visible above the background. However, a is clearly the unique axis and the diffraction pattern can best be fitted using $P2_1/b11$, which is the highest symmetry monoclinic subgroup of *Pbnm*. We note that the true symmetry is probably lower, as will be discussed later. With decreasing temperature, the monoclinic angle α increasingly deviates from 90°, reaching a minimum value of 89.971(1)° at 135 K before the trend reverses in the direction of 90°. The peak splitting requires exceptionally high resolution to resolve and is too small to detect on a laboratory powder diffractometer. The unit cell becomes metrically orthorhombic again between 35 and 55 K and the diffraction pattern can be fitted well using *Pbnm* symmetry; this confirms that the transition seen in the magnetic susceptibility at T_S=40 K is the expected change from nominal G-type to C-type OO. The susceptibility measurement suggests that this transition is first order. This is supported by our diffraction data; we observed a coexistence of both monoclinic and orthorhombic phases between 40 and ~20 K when the sample was cooled quickly through T_S. Slower cooling through T_S resulted in almost the entire sample being converted to the orthorhombic phase by 35 K. Given the suggestion of a slight cation deficiency from the TGA measurements, we refined the Ho and V fractional occupancies at low temperature. This is a difficult procedure to perform accurately due to the high degree of correlation with the isotropic displacement factors, and assuming full occupation of the oxygen sites, our best estimate was an occupancy of 0.993(6) for Ho and 0.989(7) for V. Any cation deficiency in our sample is clearly small, and subsequent refinements of the neutron diffraction data were carried out assuming the nominal stoichiometry. In order to investigate each of the different $HoVO_3$ phases observed in the XRPD and bulk magnetization measurements in greater detail, single-crystal neutron diffraction data were collected at four representative temperatures: the high-T orthorhombic phase (295 K), the monoclinic paramagnetic phase (140 K), the monoclinic magnetically ordered phase (70 K), and the low-T orthorhombic phase (20 K).

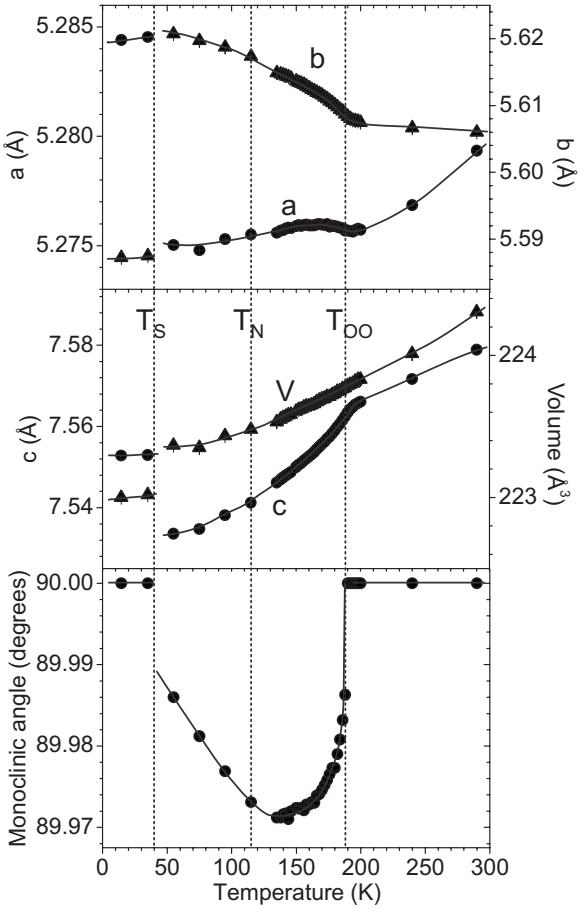

FIG. 2. Unit cell parameters and volume of $HoVO_3$ measured while heating. Positions of the structural phase transition at T_S, the magnetic ordering temperature T_N, and the orbital ordering temperature T_{OO} are indicated by vertical dotted lines. Solid lines are guides for the eyes.

A. 295 K data

A precession image of the ($h0l$) reciprocal lattice plane at 295 K based on raw data is shown in Fig. 4. Surprisingly, there appear to be weak reflections present that violate all the extinction conditions associated with the previously assumed *Pbnm* symmetry. The same is true of the ($hk0$) and ($0kl$) reciprocal lattice planes, suggesting that all the symmetry elements that give rise to the systematic extinctions in *Pbnm* have been removed. Only reflections with integral Miller in-

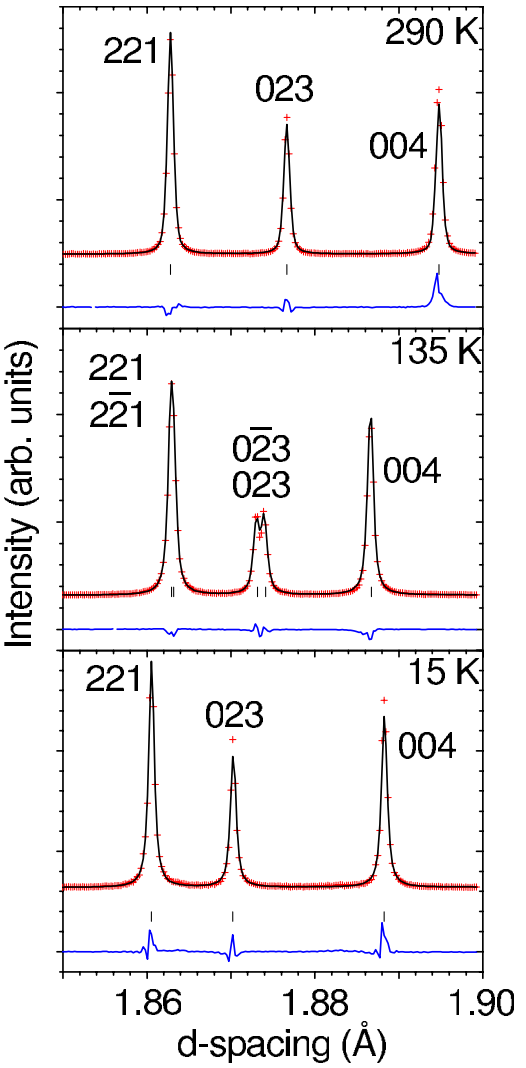

FIG. 3. (Color online) Observed (red crosses), calculated (black line), and difference (blue line) XRPD profiles of $HoVO_3$ showing splitting of peaks between 40 and 188 K due to monoclinic symmetry. Black markers indicate peak positions.

dices were observed and thus the unit cell remains the same. The highest symmetry subgroup of *Pbnm* consistent with this lack of reflection conditions is $P\bar{1}$, where only a center of symmetry is retained. Structural refinements were subsequently carried out in $P\bar{1}$, but the calculated intensities of all the weak reflections violating *Pbnm* symmetry were essentially zero; even when the possibility of pseudomerohedral twinning due to lower symmetry in a metrically orthorhombic unit cell was investigated, they could not be fitted reasonably. The structure refined using the untwinned $P\bar{1}$ model corresponded to *Pbnm* symmetry within the standard deviations of the refined parameters, including anisotropic displacement factors. The number of forbidden reflections is small (201 from a total of 9303 reflections with $I>3\sigma_I$, where I is the reflection intensity and σ_I is its standard deviation), they are weak (the intensities are all less than 0.5% of the strongest main reflections), and their intensities are not fitted and thus have essentially no effect on the refined crystal structure. Therefore, we conclude that these forbidden reflections do not originate from the average crystal structure, as discussed further in Sec. IV, and we decided to neglect them in the final analysis. The goodness of fit parameters obtained from refinement in the *Pbnm* space group was reasonable ($RwF^2=0.145$, $RF^2=0.086$, and $RF=0.047$ for 9102 reflections). A schematic picture of the V-O sublattice is shown in Fig. 5. Selected bond distances and angles are listed in Table I and the refined atomic parameters are summarized in Table II.

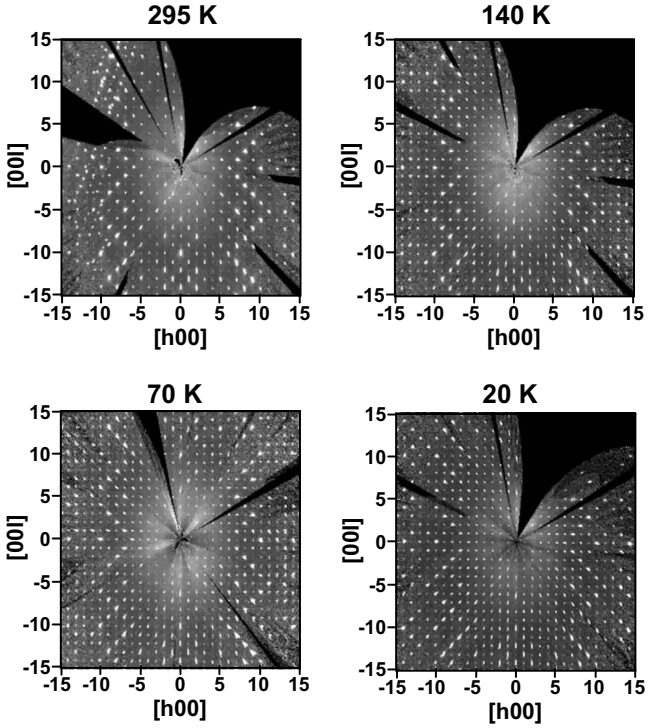

FIG. 4. Precession images extracted from raw single-crystal neutron diffraction data showing the ($h0l$) reciprocal lattice plane of $HoVO_3$.

B. 140 K data

A precession image of the ($h0l$) reciprocal lattice plane at 140 K is shown in Fig. 4. There were 638 reflections that

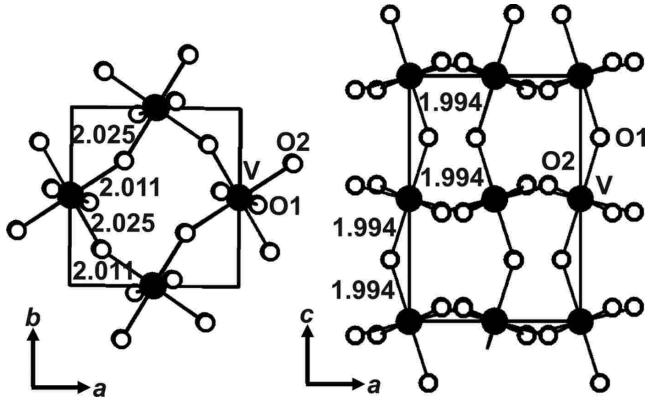

FIG. 5. Arrangement of V-O bond lengths in $HoVO_3$ at 295 K (standard errors are less than 0.001 Å). Filled circles represent V atoms and open circles represent O atoms. The unit cell is outlined.

TABLE I. Selected bond distances (Å) and angles (deg) for $HoVO_3$.

	295 K (*Pbnm*)	140 K (*Pb*11)	70 K (*Pb*11)	20 K (*Pbnm*)
Ho1-O1*a*	2.2400(2)	2.2496(5)	2.2468(5)	2.2483(2)
Ho1-O1*a*	2.3059(4)	2.2784(9)	2.2827(9)	2.2996(4)
Ho1-O2*a*	2.4963(2)×2	2.4995(7)	2.4979(6)	2.4800(2)×2
Ho1-O2*a*		2.2694(7)	2.2694(6)	
Ho1-O2*b*	2.2788(2)×2	2.2776(8)	2.2726(7)	2.2757(3)×2
Ho1-O2*b*		2.4655(6)	2.4630(6)	
Ho1-O2*c*	2.6699(2)×2	2.6488(5)	2.6415(5)	2.6670(2)×2
Ho1-O2*d*		2.6564(5)	2.6562(6)	
Ho2-O1*b*		2.2378(5)	2.2484(5)	
Ho2-O1*b*		2.3288(9)	2.3267(9)	
Ho2-O2*a*		2.6576(6)	2.6511(5)	
Ho2-O2*b*		2.6849(5)	2.6870(5)	
Ho2-O2*c*		2.4967(7)	2.5000(6)	
Ho2-O2*c*		2.2787(8)	2.2792(8)	
Ho2-O2*d*		2.2789(8)	2.2749(8)	
Ho2-O2*d*		2.4960(8)	2.4889(8)	
V1-O1*a*	1.9944(1)×2	1.9890	1.9908	1.9899(1)×2
V1-O1*b*		1.9864(4)	1.9753(3)	
V1-O2*a*	2.0254(3)×2	2.0793(10)	2.0747(10)	1.9893(2)×2
V1-O2*a*		1.9644(7)	1.9701(7)	
V1-O2*d*	2.0108(2)×2	1.9940(8)	1.9834(8)	2.0438(2)×2
V1-O2*d*		2.0364(11)	2.0478(11)	
V2-O1*a*		1.9860	1.9810	
V2-O1*b*		1.9883(3)	1.9878(3)	
V2-O2*b*		2.0642(8)	2.0691(7)	
V2-O2*b*		1.9966(11)	1.9934(10)	
V2-O2*c*		1.9856(11)	1.9934(10)	
V2-O2*c*		2.0375(8)	2.0342(7)	
V1-O1*a*-V2	143.62(1)	143.38	143.07	143.20(1)
V1-O1*b*-V2		143.40(3)	143.84(3)	

violated *Pbnm* symmetry from a total of 12 255 reflections in the data set with $I>3\sigma_I$. Of these, 510 were $h0l, h+l=2n+1$ reflections, some of which were almost an order of magnitude stronger than those at 295 K. The 128 $0kl, k=2n+1$ reflections were generally of similar intensity to those at room temperature. The XRPD data demonstrated that the highest possible symmetry in the monoclinic temperature regime is $P2_1/b11$, which is consistent with the presence of $h0l, h+l=2n+1$ reflections. It has been suggested that in the case of YVO_3 the true symmetry is lower, the structure adopting either the monoclinic subgroup *Pb*11 or the triclinic subgroup $P\bar{1}$.[35] Refinements were thus carried

TABLE II. Refined atomic coordinates and anisotropic displacement factors (Å$^2\times 100$) for $HoVO_3$ at 295 K (space group *Pbnm*).

Atom		*x*	*y*	*z*	U_{11}	U_{22}	U_{33}	U_{12}	U_{13}	U_{23}
Ho	4*c*	0.98073(2)	0.06863(4)	$\frac{1}{4}$	0.514(3)	0.624(10)	0.517(3)	−0.045(3)	0	0
V	4*b*	$\frac{1}{2}$	0	0	0.4					
O1	4*c*	0.11056(3)	0.46137(6)	$\frac{1}{4}$	0.691(4)	0.934(14)	0.486(4)	−0.083(5)	0	0
O2	8*d*	0.69148(2)	0.30378(5)	0.05600(2)	0.660(3)	0.858(12)	0.783(3)	−0.106(4)	0.087(2)	−0.126(4)

TABLE III. Refined atomic coordinates and anisotropic displacement factors ($Å^2 \times 100$) for $HoVO_3$ at 140 K (space group $Pb11$).

Atom		x	y	z	U_{11}	U_{22}	U_{33}	U_{12}	U_{13}	U_{23}
Ho1	2*a*	0.7300(1)	0.8247(2)	0.2486(1)	0.28(1)	0.46(2)	0.31(1)	−0.07(1)	0.01(1)	−0.13(1)
Ho2	2*a*	0.7701(1)	0.6856(2)	0.7480(1)	0.28(1)	0.51(2)	0.27(1)	0.03(1)	0.01(1)	−0.19(1)
V1	2*a*	$\frac{1}{4}$	$\frac{3}{4}$	0	0.3					
V2	2*a*	$\frac{1}{4}$	$\frac{3}{4}$	$\frac{1}{2}$	0.3					
O1*a*	2*a*	0.1390(1)	0.7114	0.2502	0.38(1)	1.08(4)	0.24(1)	0.12(1)	−0.06(1)	−0.25(1)
O1*b*	2*a*	0.3606(1)	0.7895(1)	0.7501(1)	0.59(1)	0.41(3)	0.46(1)	−0.02(1)	0.06(1)	−0.16(1)
O2*a*	2*a*	0.4440(1)	0.0642(2)	0.0537(1)	0.20(1)	0.49(3)	0.49(1)	0.01(1)	0.10(1)	0.04(1)
O2*b*	2*a*	0.0613(1)	0.4525(2)	0.5533(1)	0.53(1)	0.73(3)	0.40(1)	−0.36(1)	−0.05(1)	−0.16(1)
O2*c*	2*a*	0.5658(1)	0.5494(2)	0.4384(1)	0.35(1)	0.80(3)	0.59(1)	−0.09(1)	0.08(1)	0.17(1)
O2*d*	2*a*	0.9457(1)	0.9467(2)	0.9438(1)	0.76(1)	0.65(4)	0.52(1)	0.15(1)	−0.04(1)	−0.23(1)

out in all three space groups. In all cases the introduction of a twin law resulting from domains of left- and right-handed unit cells was necessary in order to obtain significant calculated intensity in the $h0l, h+l=2n+1$ reflections. This type of twinning is a natural consequence of the phase transition from *Pbnm* to one of its monoclinic subgroups and has previously been observed in YVO_3.[4] In the case of $Pb11$ and $P\bar{1}$ further twinning is possible, but the quality of fit was not improved by introducing additional twin laws, which only resulted in a decrease in the reliability of the refinement due to an increased number of correlations between refined parameters. No significant intensity could be obtained in the $0kl, k=2n+1$ reflections for any of the structural models and once again they seem to arise from other factors. Refinement in the $P\bar{1}$ space group gave a structural model where the refined parameters do not significantly deviate from those of the $P2_1/b11$ model. Thus, we could narrow the possible solutions to either $P2_1/b11$ or $Pb11$. For $Pb11$ the unit cell origin is not fixed along the *b* and *c* axes and there is only a single Wyckoff position with a multiplicity of 2. This is problematic in the case of the V atoms (which are fixed on special positions in both $P2_1/b11$ and $P\bar{1}$) since V has a low scattering cross section and is essentially invisible to neutrons. Therefore, in order to obtain realistic V-O bond lengths, we fixed the V atoms at their centrosymmetric positions and the *y* and *z* coordinates of one oxygen atom (O 1*a*) to the values obtained from the $P2_1/b11$ refinement. This approach has the effect of fixing the origin along the *b* and *c* axes and ensuring that the arrangement of the other atoms with respect to V is realistic. The disadvantage is that the V1-O1*a* distance cannot be determined. The refinement in $Pb11$ gave a marginally better fit ($RwF^2=0.147$, $RF^2=0.086$, and $RF=0.048$) than that in $P2_1/b11$ ($RwF^2=0.164$, $RF^2=0.090$, and $RF=0.051$). All refined parameters were realistic in both cases, and from the quality of the fits alone we are reluctant to conclude that $Pb11$ is the correct space group. In order to help distinguish between the two models we then checked the fits to the subset of reflections that are forbidden in *Pbnm* but allowed in both monoclinic space groups: $h0l, h+l=2n+1$. Without further refinement, which proved to be impossible due to the small number of reflections, the quality of fit was clearly better in $Pb11$ ($RwF^2=0.528$, $RF^2=0.328$, and $RF=0.214$ for 510 reflections) than in $P2_1/b11$ ($RwF^2=0.568$, $RF^2=0.392$, and $RF=0.283$). We note that these fits include 17 $h00, h=2n+1$ reflections that are allowed only in $Pb11$ and are fitted reasonably well, but they have little influence on the values of the fit parameters. It is clear that the fit parameters for the $h0l, h+l=2n+1$ subgroup are rather poor in both cases. We attribute this to the fact that all reflections in the entire data set will have an "erroneous" intensity contribution from the same origin as the forbidden $0kl$ reflections, which will be proportionally greater for weak reflections such as $h0l, h+l=2n+1$ and will thus have a detrimental effect on the goodness of fit to this subset. However, this does not affect our choice of $Pb11$ as the correct space group and has essentially no influence on the structural parameters determined using the entire data set. Selected bond distances and angles are summarized in Table I, and the refined atomic parameters are listed in Table III. The V-O bonding pattern is shown in Fig. 6.

C. 70 K data

The refinement of the 70 K data set proceeded in similar fashion to that at 140 K. From a total of 14 683 reflections with $I>3\sigma_I$ there were 123 weak $0kl, k=2n+1$ reflections with no magnetic component (see below), for which there was once again essentially no calculated intensity when models of lower symmetry than $P2_1/b11$ and $Pb11$ were checked. The fit to the entire data set was again slightly better in $Pb11$ ($RwF^2=0.143$, $RF^2=0.086$, and $RF=0.047$) than that in $P2_1/b11$ ($RwF^2=0.159$, $RF^2=0.088$, and $RF=0.049$). The difference in fit quality became more apparent when the resulting models were checked against a combination of the 678 $h0l, h+l=2n+1$ and magnetic $0kl, k=2n+1$ reflections ($RF^2=0.322$ and $RF=0.214$ for $Pb11$ versus $RF^2=0.393$ and $RF=0.295$ for $P2_1/b11$). Refinement in $P\bar{1}$ gave a fit no better than in $P2_1/b11$. Assuming that $Pb11$ is the correct symmetry, the V-O bonding pattern is similar to that at 140 K. Selected bond distances and angles are summarized in Table I, the refined atomic parameters are listed in Table IV, and the V-O bonding pattern is shown in Fig. 7. As mentioned above, additional intensity due to the magnetic contribution of the V spins was observed. In both monoclinic

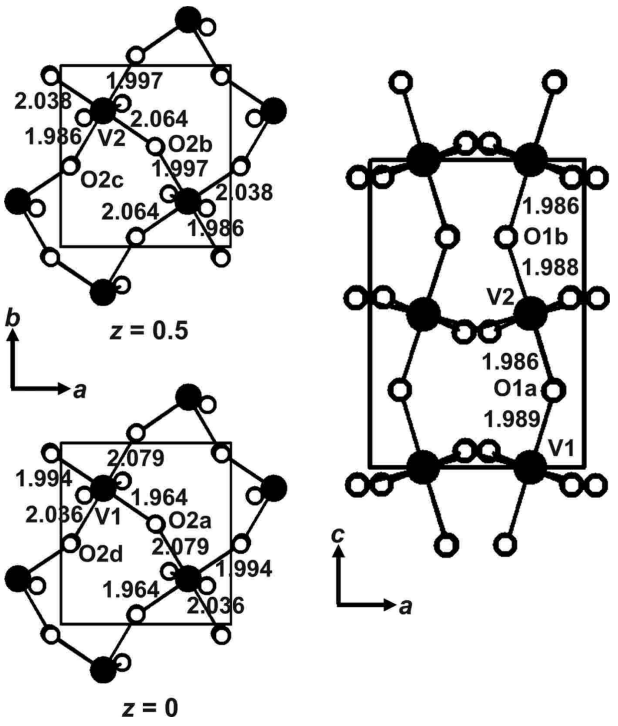

FIG. 6. Arrangement of V-O bond lengths in $HoVO_3$ at 140 K (standard errors are less than 0.002 Å).

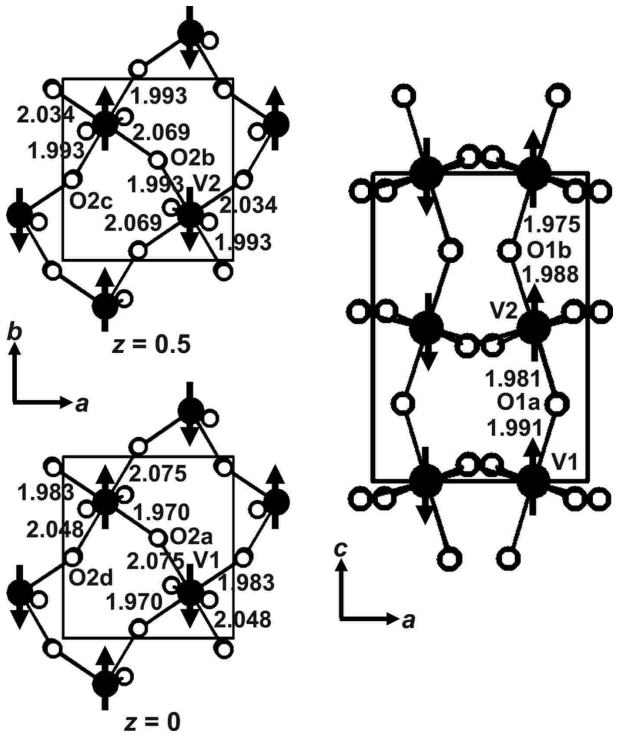

FIG. 7. Arrangement of V-O bond lengths in $HoVO_3$ at 70 K (standard errors are less than 0.002 Å). Arrows represent the directions of the V magnetic moments.

space groups there are two crystallographically independent atoms V1 and V2 located on the special positions $(0,\frac{1}{2},0)$ and $(0,\frac{1}{2},\frac{1}{2})$ for $P2_1/b11$ and fixed in our refinements at $(\frac{1}{4},\frac{3}{4},0)$ and $(\frac{1}{4},\frac{3}{4},\frac{1}{2})$ for $Pb11$. Group theoretical analysis, as described by Reehuis *et al.*,[14] shows that two ordered V-spin configurations (F_x,A_y,A_z) and (A_x,F_y,F_z) are allowed for each space group, where the modes A and F refer to the spin sequences (+−) and (++) for pairs of equivalent V atoms in a given ab plane. The best fit to our data was obtained for the $(0,A_y,A_z)$ configuration within the ab plane, with successive ab planes being equivalent. This corresponds to C-type AF ordering with components of the magnetic moment along each axis of $m_y=0.68(2)\mu_B$, $m_z=0.82(4)\mu_B$, and $m_{\text{total}}=1.07(2)\mu_B$, as shown schematically in Fig. 7. In contrast to our results, Reehuis *et al.*[14] reported that the V moments order in the ab plane [the $(A_x,A_y,0)$ configuration] for RVO_3 (R=Y, Tb, Nd) and that a small G-type AF component along the c axis was also present for R=Y. As the authors point out, this spin configuration is incompatible with $Pb11$ or $P2_1/b11$ symmetry without including biquadratic spin-spin interactions in the spin Hamiltonian; these are negligible in the majority of magnetically ordered materials. We tested the viability of the "forbidden" $(A_x,A_y,0)$ and (A_x,A_y,A_z) spin configurations in our $HoVO_3$ data but m_x refined to zero in both cases. Furthermore, the 101 and 011 reflections characteristic of G-type AF ordering had zero magnetic intensity within errors; any G-type magnetic component that might be present is thus below the sensitivity of our measurement and certainly much smaller than the value of $0.30\mu_B$ reported for

TABLE IV. Refined atomic coordinates and anisotropic displacement factors (Å$^2\times 100$) for $HoVO_3$ at 70 K (space group $Pb11$).

Atom		x	y	z	U_{11}	U_{22}	U_{33}	U_{12}	U_{13}	U_{23}
Ho1	2a	0.7297(1)	0.8242(2)	0.2491(1)	0.26(1)	0.22(2)	0.28(1)	−0.13(1)	0.04(1)	−0.11(1)
Ho2	2a	0.7705(1)	0.6846(2)	0.7489(1)	0.17(1)	0.70(2)	0.16(1)	0.11(1)	−0.01(1)	−0.22(1)
V1	2a	$\frac{1}{4}$	$\frac{3}{4}$	0	0.2					
V2	2a	$\frac{1}{4}$	$\frac{3}{4}$	$\frac{1}{2}$	0.2					
O1a	2a	0.1382(1)	0.7110	0.2507	0.28(1)	0.71(3)	0.25(1)	0.10(1)	−0.03(1)	−0.15(1)
O1b	2a	0.3590(1)	0.7888(1)	0.7509(1)	0.49(1)	0.53(3)	0.32(1)	−0.09(1)	0.03(1)	−0.22(1)
O2a	2a	0.4436(1)	0.0631(2)	0.0541(1)	0.18(1)	0.34(3)	0.43(1)	−0.02(1)	0.06(1)	0.02(1)
O2b	2a	0.0615(1)	0.4510(2)	0.5534(1)	0.36(1)	0.49(3)	0.32(1)	−0.23(1)	−0.03(1)	−0.11(1)
O2c	2a	0.5664(1)	0.5488(2)	0.4382(1)	0.34(1)	0.75(3)	0.42(1)	0.01(1)	0.12(1)	0.08(1)
O2d	2a	0.9470(1)	0.9451(2)	0.9441(1)	0.57(1)	0.72(4)	0.41(1)	0.04(1)	−0.08(1)	−0.15(1)

TABLE V. Refined atomic coordinates and anisotropic displacement factors ($Å^2 \times 100$) for $HoVO_3$ at 20 K (space group *Pbnm*).

Atom		*x*	*y*	*z*	U_{11}	U_{22}	U_{33}	U_{12}	U_{13}	U_{23}
Ho	4*c*	0.97847(2)	0.06984(4)	$\frac{1}{4}$	0.210(2)	0.393(8)	0.216(2)	−0.012(3)	0	0
V	4*b*	$\frac{1}{2}$	0	0	0.2					
O1	4*c*	0.11173(3)	0.46164(7)	$\frac{1}{4}$	0.387(3)	0.643(13)	0.332(3)	−0.034(4)	0	0
O2	8*d*	0.68692(3)	0.29939(5)	0.05670(2)	0.392(3)	0.566(10)	0.450(3)	−0.044(3)	0.034(2)	−0.051(3)

YVO_3. Our magnetic symmetry also allows the presence of an F_x mode. This means that the V spins can be canted to give a small net FM moment along the *a* axis. Although our neutron data are not sensitive to magnetic moments below $\sim 0.1 \mu_B$, the large *a*-axis magnetic susceptibility below T_N in Fig. 1 suggests that there might indeed be a small FM component along *a*. Further magnetization measurements would be required to confirm this. The reason for the discrepancy between our results and those of Reehuis *et al.* is unclear. In particular, there is no obvious reason why YVO_3 and $HoVO_3$ should have such different magnetic structures (the ionic radii of Y^{3+} and Ho^{3+} are similar). It is possible that the large single-ion anisotropy of the Ho^{3+} ion has a strong influence, even in the monoclinic phase where the Ho spins are not yet ordered.

D. 20 K data

Refinement of the 20 K data set was first carried out in the $P\bar{1}$ space group due to the lack of systematic extinctions (Fig. 4), which gave a structural model where the refined atomic coordinates and anisotropic displacement factors corresponded to *Pbnm* symmetry within their standard deviations. Refinement in *Pbnm* gave a fit with $RwF^2=0.180$, $RF^2=0.097$, and $RF=0.054$ for 15 045 reflections with $I > 3\sigma_I$. There is an alternating pattern of long and short V-O bonds in the *ab* plane indicative of the JT distortion associated with *C*-type OO. Selected bond distances and angles are listed in Table I, the refined atomic parameters are given in Table V, and the V-O bonding pattern is shown in Fig. 8. There is a strong magnetic contribution to the reflection intensities, including many in the forbidden $h0l, h+l=2n+1$ and $0kl, k=2n+1$ subsets. The magnetic structure at 20 K was solved with the help of the 5 K neutron powder diffraction data collected on HRPD. The powder and single-crystal data are complementary; although more accurate information can be extracted from single-crystal data over most of the reciprocal lattice, the intensities of magnetic reflections above ~4 Å were obtained with greater precision from the powder data due to a better modeling of the absorption at high *d* spacings. A preliminary magnetic model was obtained from the 5 K powder data, which was then used as a starting point in refinements using the 20 K single-crystal data. In *Pbnm* symmetry, group theoretical analysis[14] shows that all the possible antiferromagnetic and ferromagnetic modes are restricted to one of the crystal axes for both the V and Ho sites. The best fit was obtained when the V spins order in the expected *G*-type AF fashion with $m_z=1.36(4)\mu_B$ at 20 K, as shown schematically in Fig. 8. The magnetic transition at T_S thus involves a rotation of the V spins in the *bc* plane toward the *c* axis, as required by the *Pbnm* symmetry of the *C*-type OO phase. The Ho spins are already substantially ordered at 20 K and lie in the *ab* plane. They are arranged in a strongly canted *C*-type AF configuration with a ferromagnetic component of $m_x=1.98(3)\mu_B$ and an AF component of $m_y=4.57(2)\mu_B$, giving a total ordered moment of $4.98(2)\mu_B$. The magnetic structure at 5 K obtained from the powder data is similar. The ordered V moment was fixed at the reasonable value of $m_z=1.50\ \mu_B$ since the moments of V and Ho are highly correlated; ordered Ho moments of $m_x=3.10(2)\mu_B$, $m_y=6.81(2)\mu_B$, and $m_{\text{total}}=7.48(2)\mu_B$ were then obtained.

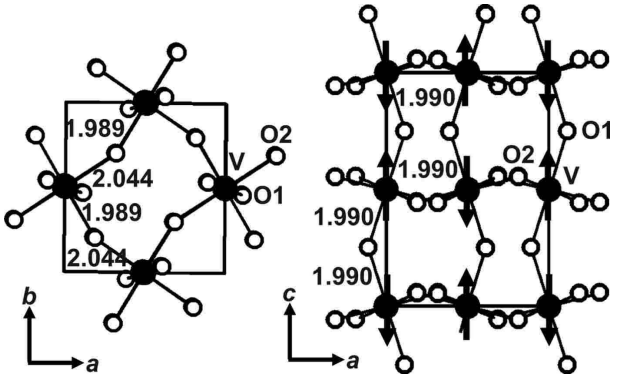

FIG. 8. Arrangement of V-O bond lengths in $HoVO_3$ at 20 K (standard errors are less than 0.001 Å). Arrows represent the directions of the V magnetic moments.

IV. DISCUSSION

A detailed knowledge of the RVO_3 crystal structure is essential in order to understand the experimentally observed physical properties and in order to provide a sound base for theoretical work. However, there are few accurate structural details available on the monoclinic phase of RVO_3. This is most likely due to two main factors. First, the extremely small deviation of the monoclinic angle from 90° results in peak splitting that can only be resolved by exceptionally high resolution in powder diffraction experiments (Fig. 3) available on only a small number of instruments worldwide. Second, twinning is often prevalent in single crystals and hinders accurate structural refinement, especially below T_{OO}. We have been able to overcome these two difficulties by growing single crystals of high quality and obtaining access to both state-of-the-art synchrotron and neutron diffraction facilities. X-ray and neutron diffraction data are often highly complementary in solving subtle crystallographic problems

that involve phase transitions. In our case high-resolution XRPD was necessary in order to locate the structural phase transition temperatures and to determine accurate lattice parameters, particularly the monoclinic angle; this is necessary to establish the correct monoclinic axis in the almost metrically orthorhombic unit cell. Knowing the unique axis, we were then able to use the single-crystal neutron diffraction data to probe the true symmetry of the various phases of $HoVO_3$. This allowed an accurate determination of the atomic parameters that are involved in the phase transitions such as, in particular, the oxygen positions. The structural determination at all temperatures was complicated by the presence of "anomalous" intensity in the neutron data at positions of the reciprocal lattice where the structure factor should be zero. The origin of these forbidden reflections is unclear. Multiple scattering effects are unlikely to be significant. Weak intensity was also observed in the 001 reflection (forbidden in the *Pbnm* phases) at both 295 and 15 K when repeated scans were carried out over a limited angular range in the synchrotron XRPD experiments. Other reasons for the anomalous intensity must then be considered. For example, it is known that pronounced anharmonic thermal motion can give rise to weak diffraction intensity where the structure factor would otherwise be zero.[38] Indeed, significant anharmonicity at room temperature was found by Massa *et al.*[18] when performing infrared spectroscopy on YVO_3. However, it is currently unclear which atomic sites in the perovskite structure could give rise to strong anharmonic effects, and further investigation is necessary. We emphasize that the anomalous peak intensities contribute only small errors to the structural determinations described here.

Experimental evidence thus far suggests that all RVO_3 with R smaller than Dy can be grouped together in the same category, displaying structural phase transitions at T_{OO} (at least 60 K above T_N) and T_S (at least 20 K below T_N).[5,7] Thus, $HoVO_3$ can be directly compared with the most widely studied member of this category: YVO_3. The main issues to be addressed regarding the monoclinic phase of this group of compounds, between T_S and T_{OO}, are the relative strengths of the competing JT coupling and quantum orbital fluctuations. When JT coupling to the lattice dominates, an ordered arrangement of occupied xz and yz orbitals should be present, giving $P2_1/b11$ symmetry. When orbital fluctuations dominate to the extent that an orbitally dimerized state arises, the symmetry is expected to be lowered to $Pb11$. The optical spectroscopy investigation of Tsvetkov *et al.*[35] on YVO_3 showed that the highest possible symmetry of the phase between T_S and T_{OO} is $Pb11$ or $P\bar{1}$. Our neutron diffraction results for $HoVO_3$ agree with these findings, indicating that $Pb11$ is the correct symmetry. However, the question remains on whether we have direct structural evidence for the orbitally dimerized state. We were unable to probe shifts of the V atoms that would be a direct signature of orbital dimerization for the following reasons. First, the neutron scattering cross section of V is close to zero and so the positions and atomic displacement factors of the V atoms had to be fixed during structural refinement. Second, our synchrotron XRPD data are insensitive to V-atom shifts as they do not contain any reflections that violate centrosymmetric $P2_1/b11$ symmetry. Anisotropic displacement factors might give an indication of dimerization, but the scattering in the x-ray data is dominated by the heavy Ho atom and we were thus unable to refine them in a meaningful fashion. Therefore, indirect structural evidence must be examined. A coherently ordered arrangement of orbital singlets would have a strong influence on the average positions of the oxygen atoms surrounding each V, to which our neutron measurements are highly sensitive. In such a structure only the xy orbitals would be preferentially occupied on each V site, with the second t_{2g} electron being located in the orbital dimer. The orbital occupation would thus be effectively the same on every V site and unlike in the OO structure, no differentiation of bond distances in the ab plane would be expected other than that arising from the octahedral tilting, as seen at room temperature. At both 70 and 140 K there is clearly a strong deviation from the room temperature V-O bonding pattern in the ab plane (Figs. 6 and 7), suggesting that coherent JT coupling does occur to a significant extent. The main features of the ab-plane bonding pattern are characteristic of those expected for staggered OO along all three crystal directions, with pairs of long (>2.03 Å) and short (<2.00 Å) distances and with the pattern being out of phase in successive ab planes. Nevertheless, the average structure has $Pb11$ symmetry rather than the $P2_1/b11$ expected for G-type OO. The lowering of symmetry is mainly caused by additional shifts of the O atoms. The crystallographically equivalent pairs of long and short V-O distances in the ab plane present in $P2_1/b11$ symmetry[4] become inequivalent in $Pb11$ and do not remain equal in length. Although there are also four instead of two inequivalent V-O distances in the c direction, their values differ little from those in the $P2_1/b11$ model. Therefore, the main changes in the bonding pattern occur in the ab plane, indicating that significant orbital fluctuations perturb the underlying G-type OO. The fluctuations are clearly sufficient to break the inversion symmetry of the average structure along the b and c axes. However, they are not strong enough to lead to the extreme situation of a structure comprised of long-range ordered orbital dimers. The bonding pattern does not significantly change between 140 and 70 K, indicating that magnetic ordering has little effect on the average crystal structure. Thermal expansion data on both $HoVO_3$ (Ref. 39) and YVO_3 (Ref. 40) single crystals reveal only tiny anomalies in the lattice constants at T_N, demonstrating that the magnetic exchange striction in RVO_3 compounds with small R cations is minimal, in contrast to compounds with large R such as $CeVO_3$ and $LaVO_3$.[32,41]

Further evidence for the presence of orbital fluctuations can be found on close inspection of the neutron single-crystal diffraction precession images in Fig. 4, which reveal considerable elongation of many diffraction spots mainly in the $\mathbf{c}^*$ direction, especially for the $h0l$ reflections with low h indices. No such elongation is apparent along the $\mathbf{a}^*$ or $\mathbf{b}^*$ (not shown) axis. Although we did not observe anisotropic peak broadening in our powder diffraction data, these precession images indicate that a degree of structural disorder is present along the c axis, even at room temperature. Such anisotropy in the essentially cubic perovskite lattice is remarkable and is consistent with the presence of one-dimensional orbital fluctuations. The 295 K data suggest that significant one-

dimensional orbital correlations occur even in the high-temperature orbitally degenerate state. This is supported by the thermal conductivity measurements of Yan *et al.*[19] on several different RVO_3 compounds. In our data the elongation of reflections is largely suppressed in the *C*-type OO phase at 20 K but does not totally disappear. Although a detailed investigation of this diffuse scattering is beyond the scope of our paper, its presence is a direct indication of considerable orbital disorder along the *c* axis. This is also reflected in the small ordered V moments, only $1.07(2)\mu_B$ in the monoclinic phase at 70 K and $1.36(4)\mu_B$ at 20 K, which are much less than expected for an $S=1$ system.

The temperature dependence of the monoclinic angle α below T_{OO} is somewhat surprising; on cooling it reaches a maximum deviation from 90° at 135 K [89.971(1)°] and then gradually increases again (Fig. 2). Taking into account only JT coupling, one would expect that α is an order parameter characterizing the development of *G*-type OO, which appears to be the case in $LaVO_3$ and $CeVO_3$ (Refs. 31, 32, and 41) where the deviation of α from 90° reaches an essentially constant value shortly below T_N. However, the magnitude of the deviation from 90° is much larger in these compounds (more than 0.10°). The monoclinic angles in YVO_3 [89.979(3)° at 100 K][4] and $YbVO_3$ [89.983(3)° at 100 K][42] are much closer to 90° and similarly small to $HoVO_3$, although we have not followed them in detail as a function of temperature. We have recently carried out structural investigations of several RVO_3 compounds with intermediate-size *R* cations; the deviation of α from 90° does not smoothly increase with the radius of *R* but rather falls into two distinct ranges of 0.02°–0.03° and 0.08°–0.13°.[43] Indeed, some intermediate-*R* compounds such as $SmVO_3$ and $GdVO_3$ show a rather sharp transition between the two states. This implies that the nature of the monoclinic phase is not the same for small and large *R* cations, a notion that is supported by other reports in the literature. Optical conductivity measurements have suggested that the intermediate phase of YVO_3 is different in nature from the ground-state phase of $LaVO_3$.[15] It was subsequently argued theoretically that although $LaVO_3$ is susceptible to one-dimensional orbital fluctuations, they should largely be suppressed by considerable JT coupling, allowing the stabilization of classical *G*-type OO.[27,28] Yan *et al.*[19] measured thermal conductivity that deviated from phononlike behavior in the monoclinic phase of RVO_3 ascribed to the presence of spin and orbital fluctuations; the conductivity became more phononlike below T_N, particularly for larger-*R* compounds, suggesting that magnetic ordering increasingly suppresses the orbital fluctuations as the ionic radius of *R* increases. In the case of $LaVO_3$, where $T_N > T_{OO}$, the thermal conductivity was found to be phononlike throughout the monoclinic phase, suggesting that orbital fluctuations are weak and that JT coupling dominates. The influence of the onset of long-range magnetic ordering thus appears to be greater in the larger-*R* compounds, where significant exchange striction occurs.[32] Our structural data show that magnetic ordering in $HoVO_3$ has little or no effect on the orbital fluctuations in the monoclinic phase, which are only suppressed below T_S where fully coherent *C*-type OO is present. However, the reason for the unexpected temperature dependence of the monoclinic angle is still unclear. It may be a sensitive measure of subtle changes in the balance between JT coupling and orbital fluctuations that are not clearly reflected in the average V-O bond lengths.

A further structural feature of possible significance in $HoVO_3$ is that the octahedral distortion due to JT coupling in the monoclinic phase is not of equal magnitude in adjacent *ab* planes, even though the average V-O distance in the V1 octahedron is the same as that in the V2 octahedron to within 0.003 Å. If the long and short pairs of V-O distances in each *ab* plane are averaged (this neglects the additional O shifts due to orbital fluctuations), then the differences between the long and short bonds are 0.079 and 0.060 Å for the $z=0$ and $z=\frac{1}{2}$ planes at 140 K and 0.085 and 0.058 Å for the $z=0$ and $z=\frac{1}{2}$ planes at 70 K. This difference in JT distortion is similar to that found previously in the intermediate phase of YVO_3 (where the structure was refined in $P2_1/b11$ equivalent to averaging the bond distances in $Pb11$), where the corresponding bond length differences are 0.079 and 0.050 Å at 80 K.[4] In contrast, the monoclinic phases of $LaVO_3$ (Ref. 31) and $CeVO_3$ (Ref. 42) (also determined in $P2_1/b11$) show less difference between the JT distortions in adjacent *ab* planes. There are too few accurate structural data available on the RVO_3 monoclinic phases to state with certainty whether the difference between adjacent planes becomes more pronounced for smaller *R* cations. We note, however, that the splitting of the YVO_3 magnon spectrum observed by Ulrich *et al.*[13] and attributed to the orbital dimerized state was later reproduced by taking into account the different degrees of JT distortion in the two inequivalent *ab* planes.[28,44]

V. SUMMARY

We have carried out a detailed study of the structural properties of $HoVO_3$. At room temperature the occupied t_{2g} orbitals are not ordered in long-range fashion, although significant orbital correlations appear to be present. At 188 K a structural phase transition from orthorhombic *Pbnm* to monoclinic $Pb11$ symmetry takes place. The pattern of V-O bond lengths suggests that this is caused by a limited degree of *G*-type orbital ordering that is significantly perturbed by strong orbital fluctuations. However, the fluctuations are not strong enough to give rise to the previously predicted orbitally dimerized state. Long-range ordering of the V spins below 114 K has essentially no effect on the orbital fluctuations, which are suppressed only below a first-order transition at 40 K where *Pbnm* symmetry is regained and the orbitals fully order in *C*-type fashion.

ACKNOWLEDGMENTS

We thank R. M. Ibberson and M. Brunelli for experimental assistance at ISIS and ESRF, respectively. We are grateful to D. I. Khomskii and G. Khaliullin for stimulating discussions. This work was supported in part by the Netherlands Organisation for Scientific Research (NWO).

*Corresponding author; g.r.blake@rug.nl

[1] Y. Ren, T. T. M. Palstra, D. I. Khomskii, E. Pellegrin, A. A. Nugroho, A. A. Menovsky, and G. A. Sawatzky, Nature (London) **396**, 441 (1998).
[2] Y. Ren, T. T. M. Palstra, D. I. Khomskii, A. A. Nugroho, A. A. Menovsky, and G. A. Sawatzky, Phys. Rev. B **62**, 6577 (2000).
[3] G. R. Blake, T. T. M. Palstra, Y. Ren, A. A. Nugroho, and A. A. Menovsky, Phys. Rev. Lett. **87**, 245501 (2001).
[4] G. R. Blake, T. T. M. Palstra, Y. Ren, A. A. Nugroho, and A. A. Menovsky, Phys. Rev. B **65**, 174112 (2002).
[5] S. Miyasaka, Y. Okimoto, M. Iwama, and Y. Tokura, Phys. Rev. B **68**, 100406(R) (2003).
[6] J.-Q. Yan, J.-S. Zhou, and J. B. Goodenough, Phys. Rev. B **72**, 094412 (2005).
[7] J.-S. Zhou, J. B. Goodenough, J.-Q. Yan, and Y. Ren, Phys. Rev. Lett. **99**, 156401 (2007).
[8] J. B. Goodenough and H. C. Nguyen, Acad. Sci., Paris, C. R. **319**, 1285 (1994).
[9] H. C. Nguyen and J. B. Goodenough, Phys. Rev. B **52**, 324 (1995).
[10] M. H. Sage, G. R. Blake, G. J. Nieuwenhuys, and T. T. M. Palstra, Phys. Rev. Lett. **96**, 036401 (2006).
[11] J. B. Goodenough, Phys. Rev. **100**, 564 (1955); J. Kanamori, J. Phys. Chem. Solids **10**, 87 (1959); P. W. Anderson, Solid State Phys. **14**, 99 (1963).
[12] H. Kawano, H. Yoshizawa, and Y. Ueda, J. Phys. Soc. Jpn. **63**, 2857 (1994).
[13] C. Ulrich, G. Khaliullin, J. Sirker, M. Reehuis, M. Ohl, S. Miyasaka, Y. Tokura, and B. Keimer, Phys. Rev. Lett. **91**, 257202 (2003).
[14] M. Reehuis, C. Ulrich, P. Pattison, B. Ouladdiaf, M. C. Rheinstädter, M. Ohl, L. P. Regnault, M. Miyasaka, Y. Tokura, and B. Keimer, Phys. Rev. B **73**, 094440 (2006).
[15] S. Miyasaka, Y. Okimoto, and Y. Tokura, J. Phys. Soc. Jpn. **71**, 2086 (2002).
[16] Z. Fang, N. Nagaosa, and K. Terakura, Phys. Rev. B **67**, 035101 (2003).
[17] G. Khaliullin, P. Horsch, and A. M. Oleś, Phys. Rev. B **70**, 195103 (2004).
[18] N. E. Massa, C. Piamonteze, A. Y. Ramos, H. C. N. Tolentino, J. A. Alonso, M. J. Martínez-Lope, and M. T. Casais, Phys. Rev. B **69**, 054111 (2004).
[19] J.-Q. Yan, J.-S. Zhou, and J. B. Goodenough, Phys. Rev. Lett. **93**, 235901 (2004).
[20] G. Khaliullin, P. Horsch, and A. M. Oleś, Phys. Rev. Lett. **86**, 3879 (2001).
[21] J. Sirker and G. Khaliullin, Phys. Rev. B **67**, 100408(R) (2003).
[22] P. Horsch, G. Khaliullin, and A. M. Oleś, Phys. Rev. Lett. **91**, 257203 (2003).
[23] G. Khaliullin, Prog. Theor. Phys. Suppl. **160**, 155 (2005).
[24] A. M. Oleś, P. Horsch, and G. Khaliullin, Phys. Rev. B **75**, 184434 (2007).
[25] S. Miyasaka, S. Onoda, Y. Okimoto, J. Fujioka, M. Iwana, N. Nagaosa, and Y. Tokura, Phys. Rev. Lett. **94**, 076405 (2005).
[26] S. Sugai and K. Hirota, Phys. Rev. B **73**, 020409(R) (2006).
[27] Y. Motome, H. Seo, Z. Fang, and N. Nagaosa, Phys. Rev. Lett. **90**, 146602 (2003).
[28] Z. Fang and N. Nagaosa, Phys. Rev. Lett. **93**, 176404 (2004).
[29] M. De Raychaudhury, E. Pavarini, and O. K. Andersen, Phys. Rev. Lett. **99**, 126402 (2007).
[30] P. Horsch, A. M. Oleś, L. F. Feiner, and G. Khaliullin, Phys. Rev. Lett. **100**, 167205 (2008).
[31] P. Bordet, C. Chaillout, M. Marezio, Q. Huang, A. Santoro, S.-W. Cheong, H. Takagi, C. S. Oglesby, and B. Batlogg, J. Solid State Chem. **106**, 253 (1993).
[32] Y. Ren, A. A. Nugroho, A. A. Menovsky, J. Strempfer, U. Rütt, F. Iga, T. Takabatake, and C. W. Kimball, Phys. Rev. B **67**, 014107 (2003).
[33] A. Muñoz, J. A. Alonso, M. T. Casais, M. J. Martínez-Lope, J. L. Martínez, and M. T. Fernández-Díaz, J. Mater. Chem. **13**, 1234 (2003).
[34] A. Muñoz, J. A. Alonso, M. T. Casais, M. J. Martínez-Lope, J. L. Martínez, and M. T. Fernández-Díaz, Chem. Mater. **16**, 1544 (2004).
[35] A. A. Tsvetkov, F. P. Mena, P. H. M. van Loosdrecht, D. van der Marel, Y. Ren, A. A. Nugroho, A. A. Menovsky, I. S. Elfimov, and G. A. Sawatzky, Phys. Rev. B **69**, 075110 (2004).
[36] A. C. Larson and R. B. von Dreele, Los Alamos National Laboratory LAUR Report No. 86-748, 2004 (unpublished).
[37] L. D. Tung, Phys. Rev. B **73**, 024428 (2006).
[38] J. B. Roberto, B. W. Batterman, and D. T. Keating, Phys. Rev. B **9**, 2590 (1974).
[39] M. Sikora, C. Marquina, M. R. Ibarra, A. A. Nugroho, and T. T. M. Palstra, J. Magn. Magn. Mater. **316**, e692 (2007).
[40] C. Marquina, M. Sikora, M. R. Ibarra, A. A. Nugroho, and T. T. M. Palstra, J. Magn. Magn. Mater. **290-291**, 428 (2005).
[41] J.-S. Zhou, Y. Ren, J.-Q. Yan, J. F. Mitchell, and J. B. Goodenough, Phys. Rev. Lett. **100**, 046401 (2008).
[42] G. R. Blake, A. A. Nugroho, J. F. Mitchell, H. Zheng, and T. T. M. Palstra (unpublished).
[43] M. H. Sage, G. R. Blake, C. Marquina, and T. T. M. Palstra, Phys. Rev. B **76**, 195102 (2007).
[44] I. V. Solovyev, Phys. Rev. B **74**, 054412 (2006).